Environmental Science and Pollution Research (2023) 30:75156–75169
https://doi.org/10.1007/s11356-023-27604-y

RESEARCH ARTICLE

Enhancement of 15% calcium oxide doped nano zero-valent iron on arsenic removal from high-arsenic acid wastewater

Yanli Kong[1,2] · Bingjie Xu[3] · Fan Lu[3] · Zhao Han[3] · Jiangya Ma[1,2] · Zhonglin Chen[4] · Jimin Shen[4]

Received: 25 December 2022 / Accepted: 9 May 2023 / Published online: 22 May 2023

Abstract

Nano zero-valent iron (nZVI) has a great potential for arsenic removal, but it would form aggregates easily and consume largely by H^+ in the strongly acidic solution. In this work, 15%CaO doped with nZVI (15%CaO-nZVI) was successfully synthesized from a simplified ball milling mixture combined with a hydrogen reduction method, which had a high adsorption capacity for As(V) removal from high-arsenic acid wastewater. More than 97% As(V) was removed by 15%CaO-nZVI under the optimum reaction conditions of pH 1.34, initial As(V) concentration 16.21 g/L, and molar ratio of Fe/As (n_{Fe}/n_{As}) 2.5:1. The effluent pH solution was weakly acidic 6.72, and the secondary arsenic removal treatment reduced the solid waste and improved arsenic grade in slag from the mass fraction of 20.02% to 29.07%. Multiple mechanisms including Ca^{2+} enhanced effect, adsorption, reduction, and co-precipitation coexisted for As(V) removal from high-arsenic acid wastewater. Doping of CaO might lead to improving cracking channels which was benefit for electronic transmission and the confusion of atomic distribution. The in situ weak alkaline environment generated on the surface of 15%CaO-nZVI would increase the content of γ-Fe_2O_3/Fe_3O_4, which was in favor for As(V) adsorption. In addition, H^+ in the strongly acidic solution could accelerate corrosion of 15%CaO-nZVI and abundant fresh and reactive iron oxides continuously generated, which would provide plenty specific reactive site and fast charge transfer and ionic mobility for arsenic removal.

Keywords Calcium oxide doped nano zero-valent iron · High-arsenic acid wastewater · Optimized experimental conditions · Secondary arsenic removal treatment · Mechanisms

Introduction

High arsenic-containing acidic wastewater and waste residue are increasingly entering the environment without effective treatment with the development of non-ferrous metal smelting technology (Chai et al. 2016). Arsenic (As) is a typical high toxic metalloid and found in water due to its environmentally mobile property, causing serious pollution to the environment and affecting millions of people worldwide (Guan et al. 2012). High-arsenic acid wastewater is characterized by extremely high arsenic and sulfuric acid content, which contains 0.5–30 g/L arsenic and 10–200 g/L sulfuric acid with the pH lower than 1 (Li et al. 2020a, b). The disabled disposal of the arsenic-bearing wastewater had caused numerous serious contaminate water sources. What is more, the maximum arsenic concentration has been stipulated to be 10 μg/L by the Standards for Drinking Water Quality in China. Thus, the safe disposal technology for arsenic removal from high-arsenic acid wastewater has become a key issue of global concern.

Current methods for arsenic removal from waste acids included lime, ferric salt, and sulfide precipitation (Alka et al. 2021). Nevertheless, it is notable that these methods still suffered from some shortcomings, such as additional amount of alkaline reagent to control a suitable pH

Responsible Editor: Tito Roberto Cadaval Jr

✉ Zhao Han
hanzhao3208@163.com

1 School of Civil Engineering and Architecture, Anhui University of Technology, Maanshan 243002, Anhui, China

2 Engineering Research Center of Biomembrane Water Purification and Utilization Technology, Ministry of Education, Maanshan 243002, Anhui, China

3 School of Metallurgical Engineering, Anhui University of Technology, Maanshan 243002, Anhui, China

4 State Key Laboratory of Urban Water Resources and Environment, School of Municipal & Environmental Engineering, Harbin Institute of Technology, Harbin 150090, China

surrounding; the treated solid waste with high arsenic content could lead to a serious secondary pollution during the transportation, storage, and disposal due to its high solubility and leachability. All of those shortcomings challenge the industrial application (Chai et al. 2018). Thus, an alternative technique for high-arsenic acid wastewater treatment with high efficiency and low consumption should be developed. Iron-based material was a majority of technologies used for arsenic removal, and iron plays important roles for controlling arsenic speciation, distribution, and immobilization (Wang et al. 2021). In particular, nanoscale zero-valent iron (nZVI) consists of the core–shell structure, a metallic iron core encapsulated by a thin iron oxide-hydroxide shell, which can degrade and separate a wide range of environmental contaminants, especially for treating wastewater containing heavy metals (Li et al. 2014). However, the high surface energy, magnetic forces, and van der Waals type interactions limited their mobility by aggregation and sedimentation, which strongly affected the contaminant removal efficiency by nZVI (Suazo-Hernández et al. 2019). In recent years, researchers have found that surface modification and loading can improve the mobility of nZVI, enhanced contaminant removal efficiency by nZVI, reduced the release of arsenic from arsenic-loaded nZVI, and prevent the occurrence of widespread environmental pollution (Li et al. 2018).

Previous studies showed that calcium was in favor of arsenic removal and inhibited arsenic desorption from water treatment residuals. The presence of calcium, especially calcium oxide (CaO), could effectively improve the removal rate of arsenic by nZVI and stabilized arsenic in mine tailings. The results noted that lower arsenic concentration in the leachate at a pH range of 3–6 was observed when $Ca(OH)_2$ rather than NaOH was used for pH adjustment (Camacho et al. 2009). Tan et al. reported calcium silicate coated-nZVI/biochar production for As(V) removal and revealed the mechanism of enhanced nZVI activity by Ca^{2+} for As(V) removal that a protective layer of Ca_2SiO_4 would form on the surface of nZVI during the co-pyrolysis process to prevent the passivation of nZVI which would be continuously detached to expose the fresh surface of nZVI, providing more redox activity and adsorption sites (Tan et al. 2022). Moreover, it has been reported that Ca^{2+} could be adsorbed on hydrated iron oxide to form $CaCO_3$ as a nucleation precursor for the growth of iron oxide particles, and arsenic could be co-precipitated through the $CaCO_3$ surface coverage process, thereby improving the removal efficiency of arsenic and hindering the release of arsenic from nZVI (Yu et al. 2019). It had been reported that calcium showed a significant synergistic effect on the adsorption of arsenic by hydrated iron oxide (Ghosh et al. 2019). $CaCO_3$ could be used as a nucleation precursor for the growth of iron hydrated oxide particles, and these iron hydrated oxides would continuously grow outward from the precursor to form large hydrated oxide particles, which improved the removal efficiency of arsenic (Mak et al. 2009). A novel calcium-based magnetic biochar developed and iron oxide for stabilization of contamination of multiple metals were studied. The stabilization effect of calcium was elevated the solution pH, formed bi-dentate chelate, and ternary surface complexes on the surface of iron oxide and enhanced adsorption ability of porous biochar (Wu et al. 2020).

As ball milling may have an impact on contaminant removal, researchers further studied the mechanisms of ball milling enhancement on pyrite/zero-valent iron for arsenic removal in water (Du et al. 2020). The results revealed that ball milling could facilitate the electron transfer of zero-valent iron and enhanced its corrosion process; the ball-milled pyrite/zero-valent iron material possessed a higher specific surface area than ball-milled zero-valent iron. Moreover, arsenic removal processes and capacity by nZVI were directly affected by pH (Hu et al. 2022; Wang et al. 2019; Wu et al. 2017a, b), and our previous studies showed that As(V) from high-arsenic acid wastewater was significantly affected by pH, that is, nZVI surface corrosion accelerated by H^+ in the strongly acidic solution and a large amount of fresh and reactive iron oxides and oxyhydroxides were continuously generated, resulting in rapid and efficient As(V) removal through multiple mechanisms (Kong et al. 2022). Through the above research results, it can be seen that addition of calcium or activation of calcium could enhance the corrosion of the ball milling process and enhance the corrosion process of the strongly acidic solution that would synergistically improve the removal of metals such as arsenic by nZVI. Thus, arsenic removal efficiency and mechanism by a novel CaO doped nano zero-valent iron (CaO-nZVI) from high-arsenic acid wastewater aroused our interest. However, the effect of CaO-nZVI on arsenic removal from high-arsenic acid wastewater has not been addressed in the literature.

Herein, this study focused on arsenic removal efficiency and mechanism by a novel CaO doped nZVI (CaO-nZVI) from high-arsenic acid wastewater. The removal of aqueous As(V) from high-arsenic acid wastewater by CaO-nZVI through batch experiments was investigated. The objectives of this paper are (1) to investigate the efficiency of CaO-nZVI on As(V) removal from high-arsenic acid wastewater under different reaction conditions and determine of optimal synthesis parameter of CaO-nZVI and the optimal reaction conditions; (2) to evaluate and propose a novel secondary arsenic removal treatment that in order to reduce the weight of solid wastes, meanwhile further reduce its effluent As(V) concentration; and (3) to suggest the mechanisms on As(V) removal by the 15%CaO-nZVI synthesized with the optimal As(V) removal efficiency.

Materials and methods

Chemicals and reagents

All the reagents are analytical grade and used without any purification. Ferric oxide (Fe_2O_3) served as the iron source and purchased from Sinopharm Chemical Reagent Co., China. Calcium oxide (CaO), concentrated sulfuric acid (H_2SO_4), hydrochloric acid (HCl), sodium hydroxide (NaOH), methyl orange, and potassium bromate ($KBrO_3$) were purchased from Tianjin Guangfu Fine Chemical Research Institute, China. Stable nZVI and micron zero-valent iron (mZVI) were purchased from shanghai Lvyuan Chemical Co., Ltd., China. The high-arsenic acid wastewater used in the experiment was the tellurium post-precipitation solution of copper anode slime, which come from Nonferrous Metals Co., Ltd., Tongling, China. The filtrate contained 16.21 g/L As(V) with the pH 1.34. The pH of the solution was adjusted with 0.1 M HCl or NaOH as required. Each experiment was carried out in duplicate.

Synthesis of XCaO-nZVI

The synthesis process of XCaO-nZVI involved ball milling and hydrogen reduction major steps. The schematic for the synthesis of XCaO-nZVI is shown in Fig. S1. Different proportions of CaO and Fe_2O_3 were mixed for ball milling at a certain period of time (0.5 h–10 h). The mass fraction of CaO is denoted as *X*, which was the percentage of CaO in the total mass of CaO and Fe_2O_3; thus, the mixture was denoted as XCaO-Fe_2O_3. The mixture XCaO-Fe_2O_3 after ball milling was calcined by hydrogen gas for reduction under the condition of 400 °C. Then, nano zero-valent iron doped with different mass fraction of CaO was obtained and denoted as XCaO-nZVI.

Characterization and analysis

X-ray diffraction (XRD, D8ADVANCE, BRUCKNER, Germany) was used to analyze the crystal structure and mineral composition of XCaO-nZVI. The surface morphology, particle size, and elemental content distribution of XCaO-nZVI were analyzed by energy dispersive X-ray detector (SEM-XEDS, JSM-6490LV, JEOL, Japan). A Fourier transform infrared spectroscope (FTIR, Nicolet6700, Nico-let, USA) was used to evaluate the coordination of complexes after XCaO-nZVI reaction. The characterizations of surface composition and combination state of elements of XCaO-nZVI were analyzed by the X-ray photoelectron spectrometer (XPS, ESCALAB 250XI, Thermo Kalpha, USA). The concentrations of As(V) and Fe in the solutions were determined by inductively coupled plasma atomic emission spectroscopy (ICP-AES, 5300DV, Perkin Elmer, USA). The elements in the reaction filter residue were detected by X-ray Fluorescence Spectrometer (XRF, Axios, PANalytical, Netherlands). The pH values were measured by pHS-3C meter (Shanghai Leici Inc.) with potassium chloride buffer.

Batch experiments

As for As(III) removal, a certain amount of nZVI or mZVI was added to a three-port flask and then added an appropriate amount of As(III)-containing wastewater, derived from the copper anode slime after copper separation from a factory in China with the content of 11.235 g/L and the concentration H^+ 1.545 mol/L. The experimental operation process was mechanically stirring for a certain time in heat the water bath pot at a constant temperature, and then filtered with 0.45 μm filter membrane. The filtrate was constant volume, and the filter residue was vacuum dried at 105 °C for 4 h and then cooled to room temperature. The effect of reaction equilibrium time was investigated. The molar ratio of Fe/As (n_{Fe}/n_{As}) was set to 5:1, the reaction temperature and time was 70 °C and 4 h, the and the reaction kinetics was sampled at 0.1 h, 0.25 h, 0.5 h, 1.0 h, 1.5 h, 2.0 h, 2.5 h, 3.0 h, 3.5 h, and 4.0 h to obtain the reaction equilibrium time. As for the effect of molar ratio of Fe/As on As(III) removal, the molar ratio of Fe/As was 3:1, 4:1, 5:1, 6:1, 7:1, 8:1, and 9:1 respectively.

As for As(V) removal, the batch experiments were carried out using three-necked bottle in a thermostatic shaker, as shown in Fig. S1. A certain amount of XCaO-nZVI was added to 100 mL high-arsenic acid wastewater and heated in a water bath with mechanical stirring. As the mixed slurry was placed in the three-necked bottle, rapid shaking was started immediately at 200 r/min for 2 h. After each test, the slurry was filtered with a 0.45 μm membrane filter and the filtrate was diluted to 500 mL and then acidified with concentrated HNO_3 for further detection. To determine the optimal reaction conditions for As(V) from high-arsenic acid wastewater by XCaO-nZVI, the influence of quality fraction X, such as 0%, 1%, 3%, 5%, 10%, 13%, 15%, and 20%, different milling time of mixture XCaO-Fe_2O_3 0.5 h, 2 h, 4 h, 6 h, 8 h, 10 h and 20 h, and n_{Fe}/n_{As} 1:1, 1.5:1, 2:1, 2.5:1, 3:1, and 4:1, initial arsenic concentration 1 g/L, 4 g/L, 8 g/L, 12 g/L and 16.21 g/L, and the pH of 0.1, 0.30, 0.75, 1.0 and 1.34 on As(V) removal were investigated, and the specific experimental parameters are listed in Table S1. The filter residue was vacuum dried at 105 °C for 4 h and then collected after cooling to room temperature for further detection. In order to improvement of arsenic grade in slag and reduce the solid wastes, the secondary arsenic removal treatment was proposed, which was mainly reacted with the arsenic containing wastewater (As(V) = 16.21 g/L, pH = 1.34) by the

primary arsenic removal filter residue through ball milling for 300 min. The filtrate and filter residue were treated and detected according to the above method.

Results and discussion

As(III) removal by nanoscale zero-valent iron (nZVI)

Figure 1a exhibits As(III) removal efficiency by nZVI was 65.1%, which was obviously higher than that of micron zero-valent iron (mZVI) 34.1% as the reaction reached equilibrium. At this time, the residual arsenic concentration in the waste acid after arsenic removal by nZVI decreased to about 4 g/L, while that by mZVI decreased to about 7.5 g/L, which was too much higher than the limit for arsenic effluent in wastewater treatment. As shown in Fig. 1b, As(III) removal increased significantly with the increased n_{Fe}/n_{As} and the residual arsenic concentration decreased to about 3 g/L. At the same time, the concentration of H^+ in arsenic-containing waste acid decreased from 1.021 mol/L to 0.446 mol/L when n_{Fe}/n_{As} increased from 3:1 to 9:1 (Fig. 1c), indicating that most of the nZVI reacted with H^+ in waste acid, resulting in a huge waste of nZVI, and the effect of arsenic removal was not ideal. It can be further seen from Table S2 that there were 53.03% Fe and 16.97% As in the slag after the reaction of nZVI with waste acid, and the weight loss rate reached 30.471%, indicating that nZVI has high reaction activity and a large part of iron was consumed by the reaction of H^+.

The XPS spectra of Fe 2p, O 1 s, and As 3d are shown in Fig. 1d, e. As illustrated in Fig. 1d, the Fe $2p_{3/2}$ peaks of Fe(0), Fe(II), and Fe(III) were located at the binding energy of 707.1 eV, 710.2 eV, and 712.0 eV, respectively, while the binding energy of the various Fe $2p_{1/2}$ chemical state components was assigned as follows: Fe(0) 719.7 eV, Fe(II) 723.8 eV, and Fe(III) 725.6 eV (Liu et al. 2018). The peaks at 529.9 eV, 531.0 eV, and 532.0 eV in O 1 s spectrum (Fig. 1e) corresponded to the O^{2-}, OH^-, and physical adsorption or chemical binding of H_2O, respectively (Xia et al. 2017). It can be seen that there was a small amount of Fe(0) on the surface of nZVI before the reaction with waste acid. Due to the oxidation of air, most of Fe(II) and Fe(III) were formed on the surface, resulting in a small peak of Fe(0). At the same time, there were relatively large O^{2-}, OH^-, and a small amount of H_2O on the surface of nZVI. While the proportion of Fe(0) and OH^- increased after the reaction, which should be due to the waste acid made nZVI continuously corroded and dissolved, resulting Fe(0) nucleus was continuously exposed to waste acid solution and a large number of ferric hydroxides were produced that provided abundant adsorption sites for arsenic (Tuček et al. 2017). The As 3d spectrum of nZVI reacted with waste acid is shown in Fig. 1f. The peaks of As $3d_{5/2}$ at 41.6 eV, 44.03 eV, and 45.03 eV were assigned as As(0), As(V), and As(III), and the As $3d_{3/2}$ peaks of As(0), As(III), and As(V) were located at binding energies of 41.6 eV, 44.03 eV, and 45.03 eV, respectively (Ramos et al. 2009; Yan et al. 2010). Since only As(III) existed in waste acid, the result exhibited

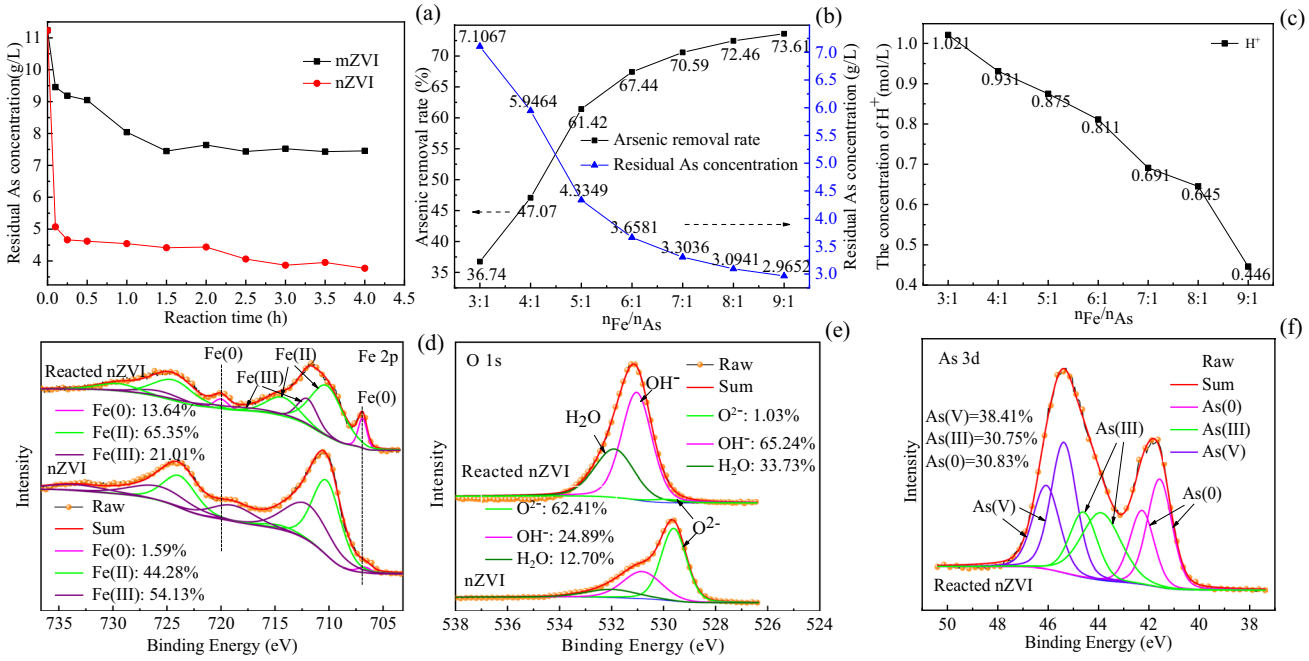

Fig. 1 As(III) removal efficiency by nZVI and mZVI (**a**). Effect of Fe/As molar ratio on As(III) removal and H^+ in solution (**b, c**) (**a–c** initial concentration of arsenic 16.21 g/L, pH = 1.34). XPS results of the slag of As(III) removal by nZVI (**d**), Fe.2p (**e**), O 1 s (**f**), and As 3d

that there were three valence states of arsenic emerged after nZVI reacted with waste acid, indicating that As(III) was not only reduced to As(0) by nZVI but also oxidized to As(V) during the reaction (Sun et al. 2011). As(III) reduced to As(0) should be due to nZVI which was continued to corrode by strongly waste acid and exposed the fresh and highly reactive zero-valent iron core. Meanwhile, the high reactivity of nZVI results in the reactions with oxygen in the air during filtration, as expressed in Eqs. (1)–(4). Both HO•·and $O_2\bullet^-$ have strong oxidation functions and combined with O_2 in the air, resulting in part of As(III) on the surface of filter residue oxidizing to As (V) (Filip et al. 2014).

$$Fe(0) + O_2 + 2H^+ \rightarrow Fe(II) + H_2O_2 \quad (1)$$

$$Fe(II) + H_2O_2 \rightarrow Fe(III) + HO\ \bullet + HO^- \quad (2)$$

$$Fe(II) + O_2 \rightarrow Fe(III) + O_2\ \bullet^- \quad (3)$$

$$Fe(III) + Fe(0) \rightarrow Fe(II) \quad (4)$$

According to the aforementioned results, nZVI has a great potential for the disposal of high-arsenic acid wastewater. Simultaneous oxidation and reduction of As(III) occurred on nZVI surfaces, and the high concentration H^+ in the strongly acidic solution accelerated nZVI surface corrosion that provided a high capacity for As(III) removal. However, due to the properties of As(III) and strongly acidic solution, nZVI could not achieve the desired adsorption performance for As(III), and a large amount of nZVI was consumed by H^+ in the waste acid, resulting in huge treated solid waste with a serious secondary pollution. In addition, arsenite is easily oxidized to arsenate, and once oxidized, several As(V)-removing technologies can be employed with more or great removal efficiency(Dong et al. 2011). Therefore, a novel train of thought was formed for direct removal of As(V) by a new high-capacity functionalized nZVI from high-arsenic acid wastewater, which make full use of H^+ and the synergistic effect of the functionalized nZVI, with the expectation to improve the quality of slag and reduce the amount of slag on the basis of improving arsenic removal efficiency.

Removal of As(V) through synergism of XCaO-nZVI

The removal efficiency of As(V) by nZVI, CaO, and 15%CaO-doped nano-zero-valent iron (15%CaO-nZVI, ball milling for 0.5 h) and the pH of filtrate after As(V) removal are shown in Fig. 2a, b, respectively. The efficiency of As(V) removal was 27.03% by nZVI, 10.53% by CaO, and 82.58% by 15%CaO-nZVI, respectively. It revealed that CaO doped nano-zero-valent iron would significantly improve As(V) removal of nZVI, indicating that some enhanced chemical reactions occurred between CaO and Fe_2O_3 during ball milling and hydrogen reduction. As shown in Fig. 2b, pH of the filtrate after As(V) removal by different materials experienced a considerable increase. CaO slightly dissolved in water formed $Ca(OH)_2$, which reacted with H^+ in solution by acid–base neutralization, thereby pH increasing by 1.06 that from 1.34 to 2.4, as expressed in Eq. (5). The nZVI might undergo redox reaction in acidic solution that leaded to pH increased by 2, as shown in Eq. (6), while the pH increased by 3.81 after As(V) removal by 15%CaO-nZVI, which was more than the sum of pH changes of As(V) by nZVI and CaO alone. It was speculated that chemical reaction occurred during CaO doped nano-zero-valent iron process. Figure 2c demonstrates that CaO quality fraction could significantly affect As(V) removal efficiency by XCaO-nZVI. The removal efficiency of As(V) increased significantly to 82.58% as CaO quality fraction increased to 15%, and it slowly increased to 83.83% with increasing CaO quality fraction to 20%. Thus, in order to reduce the amount of slag and improve the arsenic removal rate, 15% CaO-Fe_2O_3 mixture was used for ball milling-hydrogen reduction and arsenic removal in subsequent experiments.

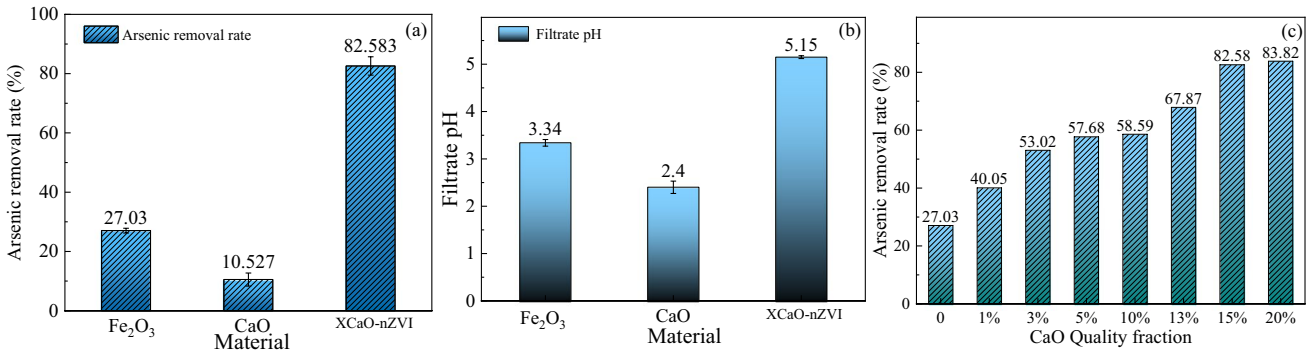

Fig. 2 As(V) removal efficiency by nZVI, CaO, and 15% CaO-doped nano-zero-valent iron (15%CaO-nZVI) (**a**); the pH of filtrate after As(V) removal (**b**); effect of CaO quality fraction on As(V) by XCaO-nZVI (**c**) (initial concentration of arsenic 16.21 g/L, pH = 1.34)

$$CaO + H_2O \rightarrow Ca(OH)_2 \quad (5)$$

$$Fe(0) + 2H^+ \rightarrow Fe2^+ + H2 \uparrow \quad (6)$$

Figure 3a–d illustrates the surface morphology and chemical composition of nZVI and 15%CaO-nZVI of using SEM and XEDS. Figure 3a shows that the pure nZVI particles were spherical with an average particle size of about 200 nm, and some agglomeration and adhesion were observed. As demonstrated in Fig. 3b, compared to the pure nZVI, the particle size of 15%CaO-nZVI decreased to about 100 nm after ball milling with doping 15% quality fraction of CaO, indicating that CaO doped would increase the friction between Fe_2O_3, making the material finer and then reducing to obtain finer 15%CaO-nZVI. The XEDS spectrum scanning was carried out in three random regions of 15%CaO-nZVI, and it was found that Ca and Fe were uniformly dispersed in each region of the material (as shown in Fig. 3c). Figure 3d shows the significant changes in the morphology of 15%CaO-nZVI after reaction with As(V). The granular and flocculent forms of the filter residue indicated that the redox reaction between 15%CaO-nZVI and As(V)-containing waste acid leads to the formation of various iron oxides. The XRD patterns of 15%CaO-nZVI after reaction with As(V) are shown in Fig. 3e. It illustrated that the newly generated granular material was mainly Fe_3O_4, and the flocculent materials might be the precursors in the transformation process of crystalline iron oxides, such as $Fe(OH)_2$ and FeOOH, which have high adsorption performance on arsenic-containing particles (Zhang et al. 2019). Interestingly, XRD patterns showed that $CaSO_4$ was generated because waste acid containing arsenic(V) was sulfuric acid system and CaO in the material was alkaline oxide, which could react with sulfuric acid to form $CaSO_4$ (Chai et al. 2018). The doping of CaO might change the surface potential of nZVI, which has an important influence the reaction with arsenic-containing particles, such as the adsorption, reduction, and co-precipitation with As(V) (Sharma et al. 2018). CaO and Fe_2O_3 reacted with water to form $Ca(OH)_2$ during ball milling, and Fe_2O_3 attached to $Ca(OH)_2$ forms XCaO-nZVI under hydrogen reduction.

Optimized experimental conditions for As(V) removal by 15%CaO-nZVI

In order to research As(V) removal mechanisms of 15%CaO-nZVI in detail, it is necessary to further improve As(V) removal efficiency, obtain the optimal conditions, and analyze the filter residue under the optimal conditions. Figure 4a shows the influence of different ball milling time on As(V) removal of 15%CaO-nZVI obtained by hydrogen reduction of 15%CaO-Fe_2O_3 mixture. Obviously, As(V) removal efficiency increased significantly with increasing ball milling time, which increased from 80.57% to 96.87% as the ball

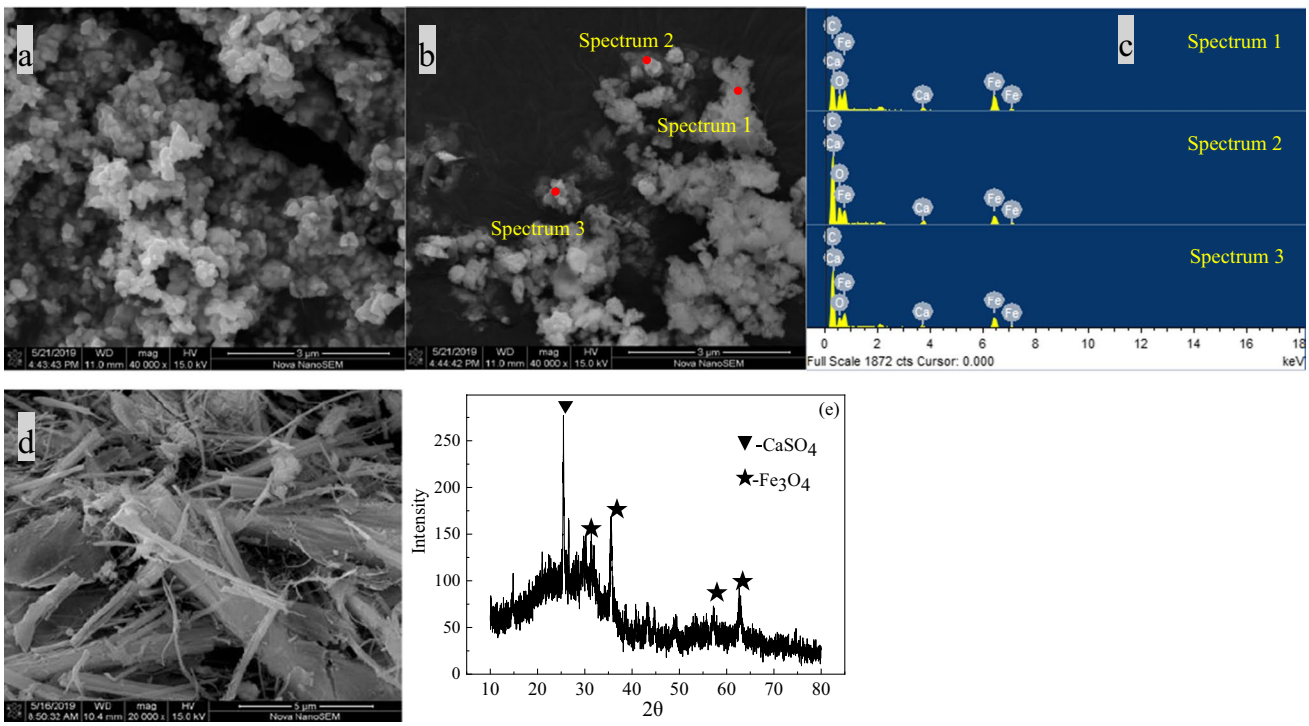

Fig. 3 SEM images of nZVI (**a**); SEM images and chemical composition of 15%CaO-nZVI (**b, c**); SEM images and XRD of 15%CaO-nZVI after reaction (**d, e**)

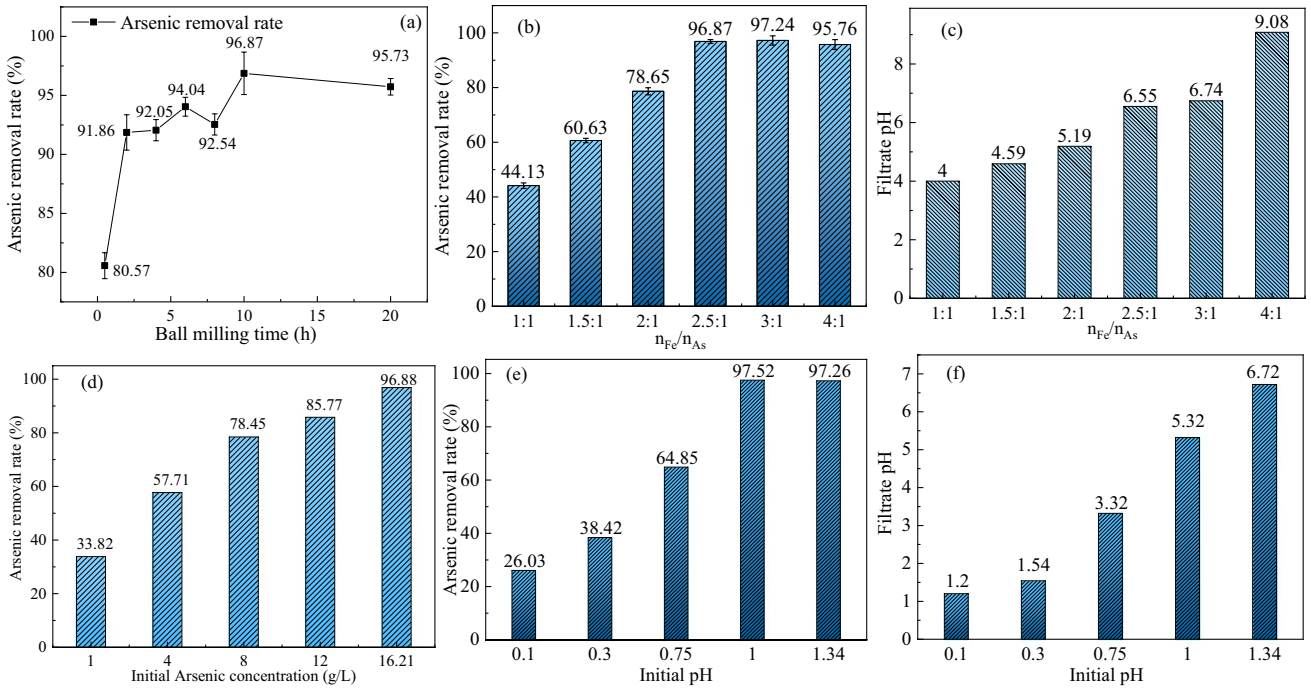

Fig. 4 Effect of ball milling time and n_{Fe}/n_{As} on As(V) removal by 15%CaO-nZVI (**a-b**); effect of n_{Fe}/n_{As} on filtrate pH (**c**) (**a–c** initial concentration of arsenic 16.21 g/L, pH = 1.34); effect of initial As(V) concentration and initial pH on As(V) removal (**d-e**); effect of initial pH on filtrate pH (**f**) (**d–f** n_{Fe}/n_{As} = 2.5:1)

milling time increased from 0.5 h to 10 h and As(V) removal rate remained almost unchanged with increasing ball milling time from 10 to 20 h. As prolongation of ball milling time would increase the process cost, taking into account both economy and effectiveness, the mixture of ball milling for 10 h was selected for subsequent experiments. Figure 4b exhibits the effect of n_{Fe}/n_{As} ratio on As(V) removal. It was obvious that As(V) removal efficiency increased rapidly from 44.13% to 96.87% as n_{Fe}/n_{As} increased from 1:1 to 2.5:1 and achieved the optimum removal effect 97.24% at n_{Fe}/n_{As} ratio 3:1, which should be attributed to increase surface area and adsorption sites (Pandey et al. 2022). Then As(V) removal efficiency experienced a gradual drop to 95.76 with n_{Fe}/n_{As} increased to 4:1, which might be due to the utilization rate of adsorbent per unit mass becomes lower (Fu et al. 2014). However, the maximal removal rate does not mean at same time optimal removal. On the one hand, As(V) was removed effectively at n_{Fe}/n_{As} 2.5:1, and the continuing increase of 15%CaO-nZVI dosage had little effect on increasing As(V), but the process cost would increase. On the other hand, the solution pH would rapidly increase as 15%CaO-nZVI increasing that the filtrate pH experienced a considerable increased from 4 to 9.08 as n_{Fe}/n_{As} increased from 1:1 to 4:1 (as illustrated in Fig. 4c). The increasing pH would cause the surface of 15%CaO-nZVI to be passivated quickly, hindering the electron transfer and inhibiting the reaction of As(V) with 15%CaO-nZVI, resulting in a decrease in As(V) removal. Thus, n_{Fe}/n_{As} of 2.5:1 was selected as the optimum value for the subsequent adsorbent experiments.

Figure 4d shows that the removal efficiency of As(V) increased significantly from 33.82% to 78.45% as the initial concentration of As(V) concentration increased from 1 g/L to 8 g/L and then experienced a gradual increase to 96.88% with increasing As(V) concentration to 16.21 g/L, the actual concentration of arsenic in the wastewater. This observation might be due to the adequate adsorption sites of 15%CaO-nZVI, and the mass transfer driving force increased with As(V) initial concentration increasing. Compared with our previous research (Kong et al. 2022), arsenic removal ability of XCaO-nZVI was higher than that of nano-iron-carbon composites synthesized, indicating that XCaO-nZVI has great potential for the disposal As(V) from high-arsenic acid wastewater. Besides surface corrosion included abundant iron oxides generated which showed high affinity for As(V); it is noteworthy that the CaO doped also possessed specific functional roles for enhanced As(V) removal.

Figure 4e reveals that the aqueous phase pH of the strongly acidic solution has great effect on As(V) removal. The results showed that the removal efficiency of As(V) by 15%CaO-nZVI was only 26.03% at pH 0.1, indicating that too low pH hindered the interactions of As(V) with 15%CaO-nZVI which should be due to the 15%CaO-nZVI corrosion rate, the forms of corrosion products, and the species of As(V) in solution under

this conditions. When the solution pH was too low, 15%CaO-nZVI surface could react with H^+ violently, resulting in rapidly and intensively iron corrosion releasing into the aqueous phase; a large amount of iron oxides could not play a role in As(V) removal. Meanwhile, As(V) species existed in neutral form H_3AsO_4 and became more mobile at pH less than 2.0 (as shown in Fig.S2), and also, the adsorbed As(V) would release into the aqueous phase again at very low pH range. Interestingly, As(V) removal by 15%CaO-nZVI experienced a considerable increase from 38.42% to 97.53% as pH increased from 0.3 to 1.0 and then remained virtually stabile 97.26% at the actual solution pH 1.34. It indicated that some unique synergistic effect properties of 15%CaO-nZVI leaded to the highly effective separation and encapsulation for As(V) removal. Similarly, the filtrate pH increased rapidly from 1.2 to 6.72 as initial solution pH increased from 5% acidity to 1.34 after reacting with 2.5:1 n_{Fe}/n_{As}, as shown in Fig. 4f; that is, pH of the filtrate reached a suitable range without extra treatment, which is of great significance to industrial As(V) removal. Therefore, As(V) could be effectively removed by 15%CaO-nZVI from the highly acidic waste acid pH 1.34 and arsenic levels up to 16.21 g/L. For subsequent experiments, the mixture of ball milling was fixed to 10 h and the ratio of n_{Fe}/n_{As} was 2.5:1. Therefore, the results implicated that the 15%CaO-nZVI synthesized has tremendous potentials on As(V) removal from high-arsenic acid wastewater. It had been also reported that more than 90% of As(V) from solution (0–5.0 mg/L) was removed by microcrystalline and mesoporous calcium-containing hydrated ferric oxide (CIHIO) at 2 g/L through surface complexation, and optimal As(V) removal efficiency achieved at pH 5.0. The presence of calcium significantly increased the adsorption of arsenic by hydrated ferric oxide (HIO) (Ghosh et al. 2019).

Improvement of arsenic grade in slag by secondary arsenic removal treatment

As arsenic-bearing residues or slags would lead to a serious secondary pollution, a novel secondary arsenic removal treatment was proposed in order to reduce the weight of solid wastes and meanwhile further reduce its effluent As(V) concentration. As shown in Tables 1 and 2, the secondary arsenic removal treatment could remove arsenic effectively for high-arsenic acid wastewater and improved arsenic grade in slag; thus, the weight of solid wastes would be reduced. As shown in Table1, arsenic concentration decreased from 16.21 g/L to 5.65 with the removal rate 60.92%, Fe concentration increased from 39.9 mg/L to 280 mg/L, and pH raised from 1.34 to 2.21, indicating that arsenic removal filter slag once again played the role of arsenic removal in the process secondary arsenic removal treatment. As illustrated in Table 2, the mass fraction of Fe element in arsenic removal residue decreased from 37.78% to 32.43%, while arsenic element increased from 20.02% to 29.07%, indicating that the arsenic grade in slag was significantly improved. In the primary arsenic removal filter residue, iron oxides and adsorbed arsenic were wrapped on the surface of 15%CaO-nZVI to form Fe-As-O shell, which inhibited the reaction of Fe(0) core with arsenic-containing wastewater. In the process of secondary arsenic removal treatment, the filter residue of primary arsenic removal and arsenic-containing wastewater were continuously mixed and collided in a ball mill tank. The Fe-As-O shell was broken by the grinding ball, and the Fe(0) core continued to react with the arsenic through reduction, adsorption and co-precipitation (Du et al. 2020). Thereby, arsenic in the solution was removed and arsenic content in the filter residue increased. At the same time, part of iron oxides dissolved, resulting in increasing the iron content in the solution and reducing the Fe content in the filter residue.

Table 1 Water quality parameter changed before and after the secondary arsenic removal treatment

Water quality parameter	Before	After	As(V) removal rate
pH	1.34	2.21	–
As(V) concentration (g/L)	16.21	5.65	60.69%
Fe concentration (mg/L)	39.9	280	–

Mechanisms of As(V) removal by 15%CaO-nZVI

Morphology characterization and phase analysis of 15%CaO-nZVI

Figure 5 illustrates the surface morphology and chemical composition of 15%CaO-nZVI using SEM and XEDS, which obtained at optimized experimental conditions for As(V) removal. The morphology and chemical composition of 15%CaO-nZVI showed significant changes before and after reaction with As(V) (as illustrated in Fig. 5a, b). After reaction, the irregular flocculent and spherical particles formed, which might be the precursors in the conversion of crystalline iron oxides, such as $Fe(OH)_2$ and FeOOH (Yan et al. 2010). The XEDS scanning of different regions revealed that Fe, As, and Ca elements were present in the samples with different morphologies (as shown in Fig. 5c).

Table 2 Arsenic grade in slag by secondary arsenic removal treatment

Element (W%)	Fe	As	S	Ca	Zr	Na	Se
One filter residue	37.78	20.02	2.51	4.10	2.24	0.987	0.896
Second filter residue	32.43	29.07	1.20	1.17	1.96	3.30	1.44

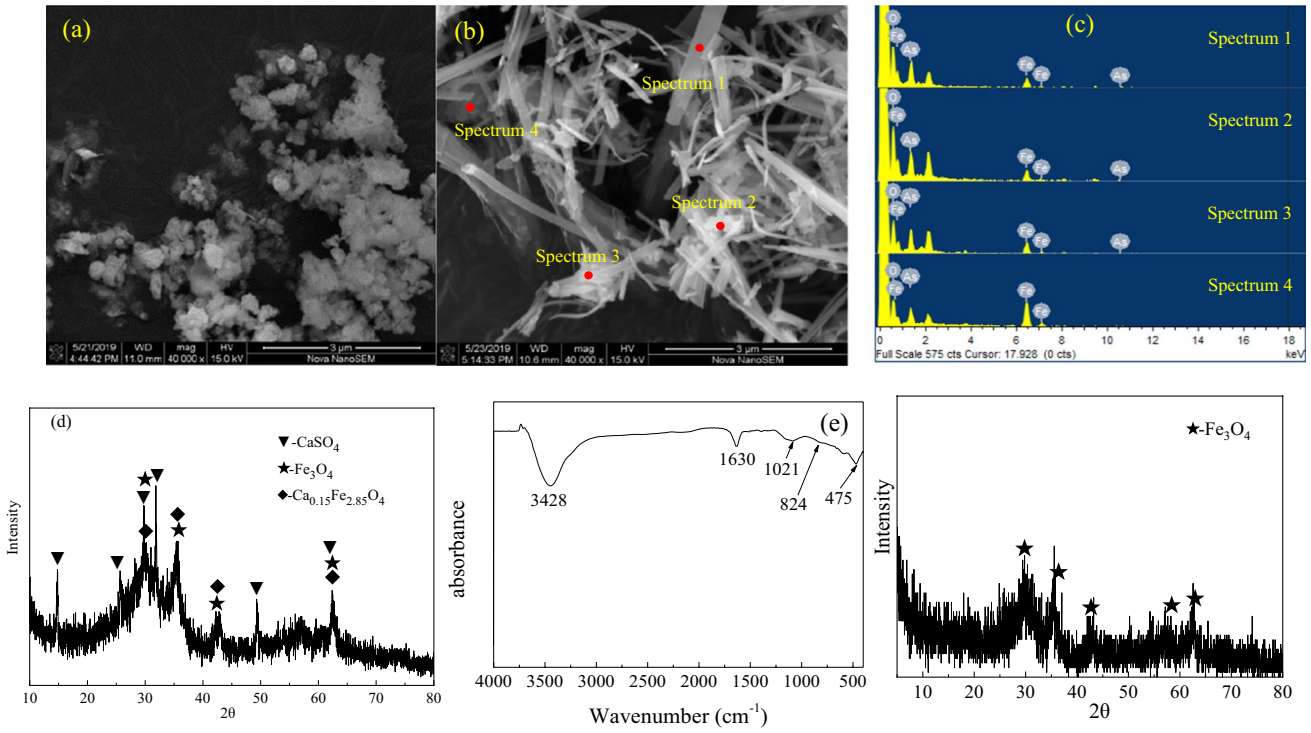

Fig. 5 SEM images of 15%CaO-nZVI before and after reaction (**a, b**); XEDS results, XRD, and FTIR spectra of 15%CaO-nZVI after reaction (**c–e**); XRD pattern of 15%CaO-nZVI after the secondary arsenic removal treatment

The XRD patterns of 15%CaO-nZVI after reaction with As(V) were shown in Fig. 5d. It showed that the main phases of arsenic-containing filter residue were $CaSO_4$, Fe_3O_4, $Ca_{0.15}Fe_{2.85}O_4$, and a large number of arsenic-containing amorphous compounds (Li et al. 2020a, b). Compared with the fresh 15%CaO-nZVI, the intensity of the reflection associated with the crystal structure of $CaSO_4$ and Fe_3O_4 changed sharply (as shown in Fig. 3e) and new mineral phases $Ca_{0.15}Fe_{2.85}O_4$ produced after adsorption reaction. The formation of $Ca_{0.15}Fe_{2.85}O_4$ might be due to the dissolution of Ca^{2+} entered the structure of corrosion products and replaced the original lattice position of iron atoms during the corrosion process. In addition, the wide diffraction peaks showed that the filter residue had poor crystallization, amorphous phase, and amorphous state, which might form amorphous compounds containing arsenic. The phase of Fe(0) was not shown, which should be attributed to $CaSO_4$, Fe_3O_4, $Ca_{0.15}Fe_{2.85}O_4$ and a large number of arsenic-containing amorphous compounds were coated on the surface of Fe(0), while XPS detection is only a few nanometers. Therefore, the following reaction might occur between 15%CaO-nZVI and As(V) in strong acidic solution, as expressed in Eqs. (7)–(14).

$$Ca(OH)_2(s)+H_2SO_4(aq) \rightarrow CaSO_4(aq)+2H_2O(l) \quad (7)$$

$$H_3AsO_4(aq)+Fe^0(s)+2H^+(aq) = Fe^{2+}(aq)+H_3AsO_3(aq)+H_2O(l) \quad (8)$$

$$Fe^0(s)+2H_2O(l) \rightarrow 2Fe^{2+}(aq)+H_2(g)+ 2OH^-(aq) \quad (9)$$

$$Fe^0(s)+O_2(g)+2H_2O(l) \rightarrow 2Fe^{2+}(aq)+ 4OH^- (aq) \quad (10)$$

$$6Fe^{2+}(aq)+O_2(g)+6H_2O(l) \rightarrow 2Fe_3O_4(s)+12H^+(aq) \quad (11)$$

$$Fe^{2+}(aq)+1/4O_2(g)+H^+(aq) \rightarrow Fe^{3+}(aq)+1/2H_2O(l) \quad (12)$$

$$Fe^{2+}(aq)+ 2OH^- (aq) \rightarrow 2Fe(OH)_2(s) \quad (13)$$

$$6Fe(OH)_2(s)+O_2(g) \rightarrow 2Fe_3O_4(s)+6H_2O(l) \quad (14)$$

Figure 5e shows the distinct surface functional groups of 15%CaO-nZVI after reaction with As(V) using FTIR spectra. The signal of peaks at 3428 cm^{-1} and 1630 cm^{-1} increased was assigned to the stretching vibration of hydroxyl groups (Li et al. 2020a, b). The characteristic vibration peak of Fe–O at 475 cm^{-1} indicated that a large number of iron oxides appeared in the filter residue (Wu et al. 2019), consistent with the result of XRD. The strong adsorption peak at 601 cm^{-1} was related to magnetite stretching vibration, while the slight

M-OH vibration peak appeared at 1021 cm^{-1}, and unique band at 824 cm^{-1} represented the vibration of As-O groups (Balladares et al. 2018). The pH of the solution increased from 1.34 to 6.72 during reaction process (as shown in Fig. 4f), indicating that the iron oxides generated on the surface of 15%CaO-nZVI were accompanied by a large number of hydroxyl groups (Asmel et al. 2017). In the high-arsenic acid wastewater, H_3AsO_4 and $H_2AsO_4^-$ exchanged with some hydroxyl groups on the surface of the iron oxides, resulting in As(V) complexing on the surface of the iron oxides, and the exchanged hydroxyl groups also increased the solution pH (Guo et al. 2016).

The XRD patterns of residue obtained from the secondary arsenic removal treatment are shown in Fig. 5f. Compared with the primary arsenic removal filter residue, the intensity of the reflection associated with $CaSO_4$ and $Ca_{0.15}Fe_{2.85}O_4$ disappeared, and only Fe_3O_4 was observed in the secondary arsenic removal filter residue. When pH < 7, the solubility of $CaSO_4$ increased with the decrease of pH, and the following reaction expressed in Eq. (15) occurred. The final pH was 6.72 after the primary arsenic removal (as shown in Fig. 4f), which was suitable for the existence of $CaSO_4$ and $Ca_{0.15}Fe_{2.85}O_4$. While the final pH was 2.21 for the secondary removal of arsenic treatment (as shown in Table 1), the solubility of $CaSO_4$ and $Ca_{0.15}Fe_{2.85}O_4$ was increased; therefore, no $CaSO_4$ and $Ca_{0.15}Fe_{2.85}O_4$ were found in the secondary arsenic removal residue, and the content of Ca in the residue was decreased (as shown in Table 2).

$$CaSO_4 + 2H^+ = Ca^{2+} + HSO_4^- \quad (15)$$

Speciation analysis of 15%CaO-nZVI after adsorption

Figure 6a shows the Eh–pH diagram for Fe-As-H_2O system in aqueous solution. Generally, the oxidation state of arsenic species played a significant role in As(V) removal, which was strongly influenced by pH. As shown in Fig. 6a, the species of H_3AsO_3, $H_2AsO_3^-$, $HAsO_3^{2-}$, AsO_3^{3-}, H_3AsO_4, $H_2AsO_4^-$, $HAsO_4^{2-}$, AsO_4^{3-}, AsH_3, Fe, Fe^{2+}, Fe^{3+}, $Fe(OH)_2$, $Fe(OH)_3$, $FeAsO_4$, and other components could be produced during Fe-As-H_2O system (Cheng et al. 2009). The theoretical stable region of ferric arsenate was 0.06 < pH < 4.54; that is, in this pH range, when the potential was higher, iron arsenate would be generated in the solution. Moreover, Fe(0) could be reduced from As(V) to As(III) and As(III) to As(0) by electron loss, while Fe(0) was oxidized to Fe(II) and Fe(III) (Ling and Zhang 2017). In our previous study, As(V) would further be reduced to As(III) and As(0) by nano-iron-carbon composites and Fe(0) was oxidized to iron oxides that possessed a high chemical reduction potential gradient driving force for arsenic removal (Kong et al. 2022).

Figure 6b, c illustrates the composite of 15%CaO-nZVI after reaction with As(V) using XPS. The XPS spectrum in Fig. 6b presented the peaks of $Fe2p_{1/2}$ and $Fe\ 2p_{3/2}$. Among them, the binding energy peaks at 729.5 eV and 724 eV correspond to $Fe\ 2p_{1/2}$, and the binding energy peaks at 711 eV and 719 eV were assigned to $Fe\ 2p_{3/2}$ (Yamashita and Hayes 2008). It revealed that abundant kinds of iron oxides were generated during reaction under highly acidic wastewater conditions, such as Fe_2O_3, $Fe(OH)_3$, Fe_3O_4, and FeOOH. Combined with related research (Su et al. 2017), the iron element in filter residue existed in the form of amorphous γ-FeOOH, γ-Fe_2O_3, and crystalline Fe_3O_4, which was consistent with the XRD results. A previous study had reported that iron species distributed in the order from outside to inside of nZVI was Fe(III) oxides, a mixed Fe(III)/Fe(II), Fe(II), and then Fe(0) core, resulting in a high driving force, and favors As(V) reduction and diffusion (Liu et al. 2018; Mokete et al. 2020). Figure 6c shows the four obvious characteristic peaks were observed; among them, the binding energy peaks at 44.8 eV and 45.9 eV were belonged to the As(V) characteristic peaks, and the binding energy peaks at 43.7 eV and 44.5 eV were assigned as As(III) characteristic peaks (Liu et al. 2018). It indicated that arsenic in the filter residue existed in the form of 75.01% As(V) and 24.98% As(III). On the one hand, the presence of Ca^{2+} increased the disorder and defective effect of iron oxides; on the other hand, the presence of Ca^{2+} might strengthen the

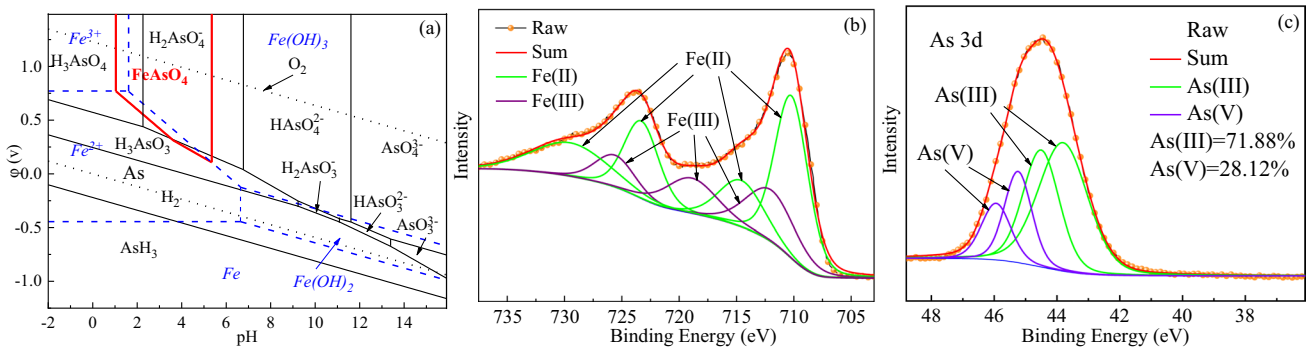

Fig. 6 Eh–pH diagram for Fe-As-H_2O system (**a**); XPS results of 15%CaO-nZVI after reaction (Fe.2p (**b**), As 3d (**c**))

channel electron transfer, which was more conducive to the reduction and immobilization of arsenic. In addition, iron oxides continuously generated in the strongly acidic industrial wastewater through intensive corrosion process (Mu et al. 2017). The adsorbed As(V) gradually diffused into the 15%CaO-nZVI particle shell, and the highly reduced Fe(0) core could reduce As(V) to As(III), while the As(V) on the surface could also co-precipitate with the iron oxides (Li et al. 2017). Therefore, As(V) could be effectively removed by 15%CaO-nZVI through various mechanisms including adsorption, reduction, and co-precipitation under high-arsenic acid wastewater conditions.

Analysis of mechanisms

The new 15%CaO-nZVI synthesized showed a very rapid and highly efficient removal of As(V) from high-arsenic acid wastewater, and the secondary arsenic removal treatment reduced the weight of solid wastes under a high As(V) removal rate. The multiple effect mechanisms were included on As(V) removal, especially the enhanced effect of 15% CaO-doped. The schematic of As(V) removal by 15%CaO-nZVI is demonstrated in Fig. 7. In the reaction process, Ca^{2+} in the 15%CaO-nZVI played important roles for enhancing As(V) removal. It could be speculated from the material morphology that the presence of CaO reduced the particle size of 15%CaO-nZVI and added some cracking channels (Mu et al. 2017). Moreover, the cracking channels increased electronic transmission and the confusion of atomic distribution, which enhancing the reduction and adsorption of As(V) (Ling et al. 2017). When 15%CaO-nZVI reacted high-arsenic acid wastewater, $Ca(OH)_2$ was easy to react with H_2SO_4 in the solution and consumed a certain amount of H^+ to form $CaSO_4$. The in situ weak alkaline environment generated on the surface of 15%CaO-nZVI reduced the content of γ-FeOOH, while the content of γ-Fe_2O_3/Fe_3O_4 increased, resulting in enhancing As(V) adsorption (Su et al. 2017). At the same time, the partially dissolved Ca^{2+} entered the corrosion product structure during the corrosion process, replacing the position of the original iron atom to generate $Ca_{0.15}Fe_{2.85}O_4$, which had stronger adsorption capacity for As(V) (Wu et al. 2017a, b). In addition, Ca^{2+} could provide more positive to promote the adsorption for As(V) (Han et al. 2017), especially the iron-calcium compounds maintained positive surface charge and prevent the leaching of negatively charged arsenic ions (Camacho et al. 2009). The H^+ in the strong acidic wastewater accelerated 15%CaO-nZVI surface corrosion rate and abundant iron oxides continuously generated. Moreover, these fresh and reactive iron corrosion products could provide plenty specific reactive site for As(V) (Xia et al. 2017). In addition, these oxygen-rich oxides were distributed on the 15%CaO-nZVI out surface; then, the inner part was reduced Fe(II) and the core was more reduced Fe(0), and the arrangement of these generated iron oxide distribution provided fast charge transfer and ionic mobility for arsenic removal (Zou et al. 2016). In the reaction process between 15%CaO-nZVI and As(V) in high-arsenic acid wastewater, As(V) could be directly adsorbed and co-precipitated on the surface of 15%CaO-nZVI, and then As(V) diffused into the reduced subsurface layer and highly reduced Fe(0) core; that is, As(V) would be reduced to As(III) and then adsorbed and co-precipitate with the iron oxides. Therefore, Multiple mechanisms including Ca^{2+} enhance effect, adsorption, reduction, and co-precipitation coexisted for As(V) removal from high-arsenic acid wastewater.

Conclusions

In this study, nano zero-valent iron doped with 15%CaO (15%CaO-nZVI) was successfully synthesized using a simplified ball milling mixture combined with hydrogen reduction method, which showed good adsorption efficiency for As(V) removal from high-arsenic acid wastewater, and was significantly higher than that of nZVI and CaO. Multiple mechanisms including Ca^{2+} enhance effect, adsorption, reduction, and co-precipitation coexisted for As(V) removal from high-arsenic acid wastewater. It was revealed that ball milling time, solution pH, adsorbent dosage, and initial As(V) concentration significantly affected As(V) removal 15%CaO-nZVI. The 15%CaO-nZVI reduced by hydrogen after ball milling for 10 h was used as the raw material. The results indicate that As(V) removal efficiency reached up to approximately 97% under the optimal As(V) removal conditions of pH 1.34, initial As(V) concentration 16.21 g/L, molar ratio of Fe/As (n_{Fe}/n_{As}) 2.5:1 at temperature 40 °C ~ 60 °C. Compared with the reaction solution pH of 1.34, the effluent solution was weakly acidic 6.72, and the mass fraction of arsenic in the arsenic removal residue was 20.02%. In order to further improve arsenic grade in slag, the secondary arsenic removal treatment was used to make the arsenic removal filter slag under the optimal conditions react with 16.21 g/L arsenic-containing wastewater again with arsenic removal rate 60.92%, and the arsenic content in the slag increased from 20.02% to 29.07%. Ca^{2+} and H^+ played important roles for enhancing As(V) removal. The presence of CaO could improve cracking channels which was benefit for electronic transmission and the confusion of atomic distribution. Moreover, Ca^{2+} could provide more positive to promote the adsorption for As(V), especially the generated iron-calcium compounds. Abundant fresh and reactive iron oxides could continuously generate by

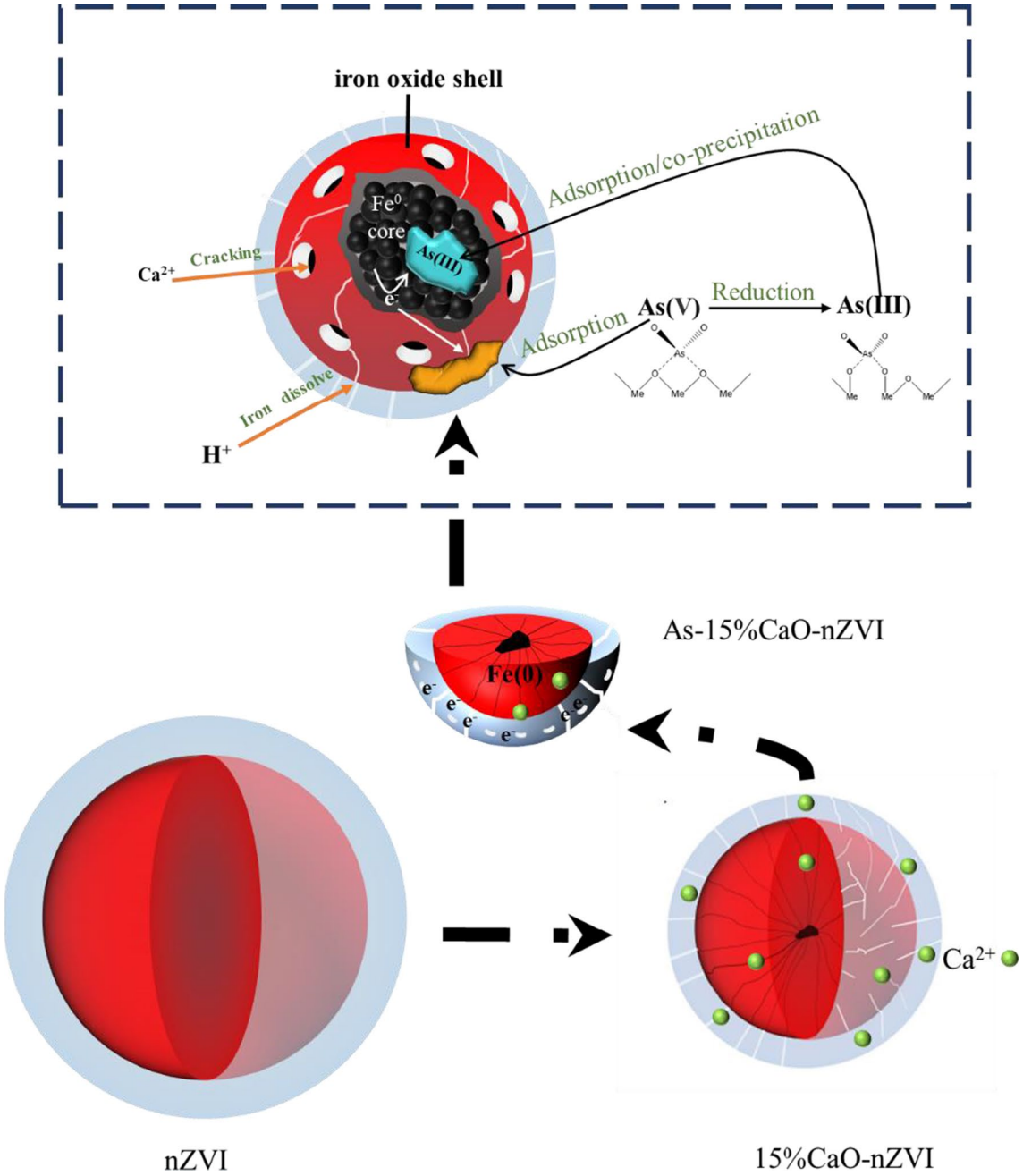

Fig. 7 Schematic of As(V) removal from high-arsenic acid wastewater by 15%CaO-nZVI

H^+ in the strongly acidic solution, which provide plenty specific reactive site and fast charge transfer and ionic mobility for arsenic removal.

Supplementary Information The online version contains supplementary material available at https://doi.org/10.1007/s11356-023-27604-y.

Author contribution Yanli Kong: conceptualization, methodology, investigation, and review and editing. Bingjie Xu: writing, formal analysis, and data curation. Fan Lu: resources, investigation, and review and editing. Zhao Han: resources, writing—review and editing, supervision, and data curation. Jiangya Ma: resources, writing—review and editing, and supervision. Zhonglin Chen: writing—review and editing. Jimin Shen: writing—review and editing.

Funding This study was supported by the Natural Science Foundation of Science and Technology Department of Anhui Province (Nos. 2008085QE242 and 2208085Y18), the Open Project of State Key Laboratory of Urban Water Resource and Environment (Harbin Institute of Technology) (No. ES201917), the Engineering Research Center of Biomembrane Water Purification and Utilization Technology (BWPU2020KF08), and the National Natural Science Foundation of China (51878001).

Data availability The datasets used or analyzed during the current study are available from the corresponding author on reasonable request.

Declarations

Ethics approval Not applicable.

Consent for publication The author agrees to publication, and the copyright to the article is transferred to the Journal of Environmental Science and Pollution Research if and when the article is accepted for publication. The author warrants that his/her contribution is original and that he/she has full power to make this grant. The author signs for and accepts responsibility for releasing this material on behalf of any and all co-authors. The copyright transfer covers the exclusive right to reproduce and distribute the article, including reprints, translations, photographic reproductions, microform, electronic form, or any other reproductions of similar nature. After submission of the agreement signed by the corresponding author, changes of authorship or in the order of the authors listed will not be accepted.

Competing interests The authors declare no competing interests.

References

Alka S, Shahir S, Ibrahim N, Ndejiko MJ, Vo DN, Manan FA (2021) Arsenic removal technologies and future trends: a mini review. J Clean Prod 278:123805

Asmel NK, Yusoff ARM, Sivarama Krishna L, Majid ZA, Salmiati S (2017) High concentration arsenic removal from aqueous solution using nano-iron ion enrich material (NIIEM) super adsorbent. Chem Eng J 317:343–355

Balladares E, Jerez O, Parada F, Baltierra L, Hernández C, Araneda E, Parra V (2018) Neutralization and co-precipitation of heavy metals by lime addition to effluent from acid plant in a copper smelter. Miner Eng 122:122–129

Camacho J, Wee H, Kramer TA, Autenrieth R (2009) Arsenic stabilization on water treatment residuals by calcium addition. J Hazard Mater 165:599–603

Chai L, Yue M, Yang J, Wang Q, Li Q, Liu H (2016) Formation of tooeleite and the role of direct removal of As(III) from high-arsenic acid wastewater. J Hazard Mater 320:620–627

Chai L, Yue M, Li Q, Zhang G, Zhang M, Wang Q, Liu H, Liu Q (2018) Enhanced stability of tooeleite by hydrothermal method for the fixation of arsenite. Hydrometallurgy 175:93–101

Cheng H, Hu Y, Luo J, Xu B, Zhao J (2009) Geochemical processes controlling fate and transport of arsenic in acid mine drainage (AMD) and natural systems. J Hazard Mater 165:13–26

Dong H, Guan X, Wang D, Li C, Yang X, Dou X (2011) A novel application of H_2O_2-Fe(II) process for arsenate removal from synthetic acid mine drainage (AMD) water. Chemosphere 85:1115–1121

Du M, Zhang Y, Zeng X, Kuang H, Huang S (2020) Enhancement of ball-miling on pyrite/zero-valent iron for arsenic removal in water: a mechanistic study. Chemosphere 249:126130

Filip J, Karlický F, Marušák Z, Lazar P, Černík M, Otyepka M, Zbořil R (2014) Anaerobic reaction of nanoscale zerovalent iron with water: mechanism and kinetics. J Phys Chem C 118:13817–13825

Fu F, Dionysiou DD, Liu H (2014) The use of zero-valent iron for groundwater remediation and wastewater treatment: a review. J Hazard Mater 267:194–205

Ghosh A, Paul S, Bhattacharya S, Sasikumar P, Biswas K, Ghosh UC (2019) Calcium ion incorporated hydrous iron(III) oxide: synthesis, characterization, and property exploitation towards water remediation from arsenite and fluoride. Environ Sci Pollut R 26:4618–4632

Guan X, Du J, Meng X, Sun Y, Sun B, Hu Q (2012) Application of titanium dioxide in arsenic removal from water: a review. J Hazard Mater 215–216:1–16

Guo X, Yang Z, Dong H, Guan X, Ren Q, Lv X, Jin X (2016) Simple combination of oxidants with zero-valent-iron (ZVI) achieved very rapid and highly efficient removal of heavy metals from water. Water Res 88:671–680

Han C, Lalley J, Iyanna N, Nadagouda MN (2017) Removal of phosphate using calcium and magnesium-modified iron-based adsorbents. Mater Chem Phys 198:115–124

Hu W, Yang L, Shao P, Shi H, Chang Z, Fang D, Wei Y, Feng Y, Huang Y, Yu K, Luo X (2022): Proton self-enhanced hydroxyl-enriched cerium oxide for effective arsenic extraction from strongly acidic wastewater. Environ Sci Technol

Kong Y, Li M, Zhou Y, Pan R, Han Z, Ma J, Chen Z, Shen J (2022) Carbothermal synthesis of nano-iron-carbon composites for arsenate removal from high-arsenic acid wastewater. J Environ Chem Eng 10:107140

Li S, Wang W, Liu Y, Zhang W (2014) Zero-valent iron nanoparticles (nZVI) for the treatment of smelting wastewater: a pilot-scale demonstration. Chem Eng J 254:115–123

Li S, Wang W, Liang F, Zhang W (2017) Heavy metal removal using nanoscale zero-valent iron (nZVI): Theory and application. J Hazard Mater 322:163–171

Li Z, Wang L, Meng J, Liu X, Xu J, Wang F, Brookes P (2018) Zeolite-supported nanoscale zero-valent iron: new findings on simultaneous adsorption of Cd(II), Pb(II), and As(III) in aqueous solution and soil. J Hazard Mater 344:1–11

Li Y, Zhu X, Qi X, Shu B, Zhang X, Li K, Wei Y, Hao F, Wang H (2020a) Efficient removal of arsenic from copper smelting wastewater in form of scorodite using copper slag. J Clean Prod 270:122428

Li Z, Wang L, Wu J, Xu Y, Wang F, Tang X, Xu J, Ok YS, Meng J, Liu X (2020b) Zeolite-supported nanoscale zero-valent iron for immobilization of cadmium, lead, and arsenic in farmland soils: encapsulation mechanisms and indigenous microbial responses. Environ Pollut 260:114098

Ling L, Zhang W (2017) Visualizing arsenate reactions and encapsulation in a single zero-valent iron nanoparticle. Environ Sci Technol 51:2288–2294

Ling L, Huang X, Li M, Zhang W (2017) Mapping the reactions in a single zero-valent iron nanoparticle. Environ Sci Technol 51:14293–14300

Liu A, Wang W, Liu J, Fu R, Zhang W (2018) Nanoencapsulation of arsenate with nanoscale zero-valent iron (nZVI): a 3D perspective. SCI BULL 63:1641–1648

Mak MSH, Rao P, Lo IMC (2009) Effects of hardness and alkalinity on the removal of arsenic(V) from humic acid-deficient and humic acid-rich groundwater by zero-valent iron. Water Res 43:4296–4304

Mokete R, Eljamal O, Sugihara Y (2020) Exploration of the reactivity of nanoscale zero-valent iron (NZVI) associated nanoparticles in diverse experimental conditions. Chem Eng Process Process Intensif 150:107879

Mu Y, Ai Z, Zhang L (2017) Phosphate shifted oxygen reduction pathway on $Fe@Fe_2O_3$ core-shell nanowires for enhanced reactive oxygen species generation and aerobic 4-chlorophenol degradation. Environ Sci Technol 51:8101–8109

Pandey K, Sharma S, Saha S (2022) Advances in design and synthesis of stabilized zero-valent iron nanoparticles for groundwater remediation. J Environ Chem Eng 10:107993

Ramos M, Yan W, Li XQ, Koel BE, Zhang WX (2009) Simultaneous oxidation and reduction of arsenic by zero-valent iron

nanoparticles: understanding the significance of the core-shell structure. J Phys Chem C 113:14591–14594
Sharma M, Ramakrishnan S, Remanan S, Madras G, Bose S (2018) Nano tin ferrous oxide decorated graphene oxide sheets for efficient arsenic (III) removal. Nano-Structures & Nano-Objects 13:82–92
Su H, Ye ZB, Hmidi N (2017) High-performance iron oxide-graphene oxide nanocomposite adsorbents for arsenic removal. Colloid Surface A 522:161–172
Suazo-Hernández J, Sepúlveda P, Manquián-Cerda K, Ramírez-Tagle R, Rubio MA, Bolan N, Sarkar B, Arancibia-Miranda N (2019) Synthesis and characterization of zeolite-based composites functionalized with nanoscale zero-valent iron for removing arsenic in the presence of selenium from water. J Hazard Mater 373:810–819
Sun F, Osseo-Asare KA, Chen Y, Dempsey BA (2011) Reduction of As(V) to As(III) by commercial ZVI or As(0) with acid-treated ZVI. J Hazard Mater 196:311–317
Tan X, Deng Y, Shu Z, Zhang C, Ye S, Chen Q, Yang H, Yang L (2022) Phytoremediation plants (ramie) and steel smelting wastes for calcium silicate coated-nZVI/biochar production: environmental risk assessment and efficient As(V) removal mechanisms. Sci Total Environ 844:156924
Tuček J, Prucek R, Kolařík J, Zoppellaro G, Petr M, Filip J, Sharma VK, Zbořil R (2017) Zero-valent iron nanoparticles reduce arsenites and arsenates to As(0) firmly embedded in core-shell superstructure: challenging strategy of arsenic treatment under anoxic conditions. ACS Sustain Chem Eng 5:3027–3038
Wang A, Zhou K, Zhang X, Zhou D, Peng C, Chen W (2019) Reductive removal of arsenic from waste acid containing high-acidity and arsenic levels through iodide and copper powder synergy. Chem Eng J 373:23–30
Wang P, Fu F, Liu T (2021) A review of the new multifunctional nano zero-valent iron composites for wastewater treatment: emergence, preparation, optimization and mechanism. Chemosphere 285:131435
Wu C, Tu J, Liu W, Zhang J, Chu S, Lu G, Lin Z, Dang Z (2017a) The double influence mechanism of pH on arsenic removal by nano zero valent iron: electrostatic interactions and the corrosion of Fe0. Environ Sci Nano 4:1544–1552
Wu C, Liu WZ, Zhang J, Chu SQ, Shi ZQ, Dang Z, Lin Z (2017b) Mechanisms of synergistic removal of low concentration As(V) by nZVI@Mg(OH)(2) nanocomposite. J Phys Chem C 121:21411–21419
Wu Z, Su X, Lin Z, Owens G, Chen Z (2019) Mechanism of As(V) removal by green synthesized iron nanoparticles. J Hazard Mater 379:120811
Wu J, Li Z, Huang D, Liu X, Tang C, Parikh SJ, Xu J (2020) A novel calcium-based magnetic biochar is effective in stabilization of arsenic and cadmium co-contamination in aerobic soils. J Hazard Mater 387:122010
Xia XF, Ling L, Zhang WX (2017) Solution and surface chemistry of the Se(IV)-Fe(0) reactions: effect of initial solution pH. Chemosphere 168:1597–1603
Yamashita T, Hayes P (2008) Analysis of XPS spectra of Fe^{2+} and Fe^{3+} ions in oxide materials. Appl Surf Sci 254:2441–2449
Yan WL, Ramos M, Koel BE, Zhang WX (2010) Multitiered distributions of arsenic in iron nanoparticles: observation of dual redox functionality enabled by a core-shell structure. Chem Commun 46:6995–6997
Yu Z, Hu L, Lo IMC (2019) Transport of the arsenic (As)-loaded nano zero-valent iron in groundwater-saturated sand columns: roles of surface modification and As loading. Chemosphere 216:428–436
Zhang XD, Shi DY, Li X, Zhang YJ, Wang JJ, Fan J (2019) Nanoscale dispersing of zero-valent iron on CaCO3 and their significant synergistic effect in high performance removal of lead. Chemosphere 224:390–397
Zou Y, Wang X, Khan A, Wang P, Liu Y, Alsaedi A, Hayat T, Wang X (2016) Environmental remediation and application of nanoscale zero-valent iron and its composites for the removal of heavy metal ions: a review. Environ Sci Technol 50:7290–7304